Curvature sensor for ocular wavefront measurement

Fernando Díaz-Doutón, Jaume Pujol, Montserrat Arjona, and Sergio O. Luque

Departamento de Óptica y Optometría, Centro de Desarrollo de Sensores, Instrumentación y Sistemas (CD6), Universidad Politécnica de Cataluña, Terrassa 08222, Spain

Received February 9, 2006; revised May 9, 2006; accepted May 11, 2006; posted May 15, 2006 (Doc. ID 67897); published July 10, 2006

We describe a new wavefront sensor for ocular aberration determination, based on the curvature sensing principle, which adapts the classical system used in astronomy for the living eye's measurements. The actual experimental setup is presented and designed following a process guided by computer simulations to adjust the design parameters for optimal performance. We present results for artificial and real young eyes, compared with the Hartmann–Shack estimations. Both methods show a similar performance for these cases. This system will allow for the measurement of higher order aberrations than the currently used wavefront sensors in situations in which they are supposed to be significant, such as postsurgery eyes. © 2006 Optical Society of America

OCIS codes: 010.7350, 330.5370.

In recent years, a large number of systems have been proposed for determining the human ocular wavefront error, substantially increasing knowledge of the eye's optical performance. Today's most significant systems are based on sampling the wavefront slope across the subject's pupil and then retrieving the wave aberration function by means of a nonlinear fit to Zernike polynomials. Examples of these kinds of techniques include the laser ray tracing method[1] and the Hartmann–Shack sensor (H–S),[2,3] which has been taken as a standard for the determination of ocular aberrations. However, this kind of technique has a drawback imposed by the number of samples on the order of aberrations that can be achieved. This fact is not important while measuring young, healthy eyes, but high-order aberrations could be significant for subjects who have some kind of ocular disease or have undergone cataract or refractive surgery.[4]

Astronomical research[5] suggests that the curvature sensor[6,7] may be an alternative to the aforementioned methods. It has not yet been applied to the determination of aberration in the eye, although its application to a dynamic tear film aberration study[8] has been reported recently. The main features of this sensor are that it can potentially achieve higher-order aberrations than current methods do, in a very large dynamic range and at a lower cost. Another major advantage is its application in fast adaptive optics systems, due to the direct correlation between the sensor's signal and the deformable mirrors' curvature. Its principle relies on the local changes in intensity in the planes perpendicular to the light's propagation direction as it travels along its optical path. In paraxial approximation, these changes are governed by the irradiance transport equation:

$$k\frac{\mathrm{d}}{\mathrm{d}z}I(\mathbf{r},z) = -\nabla[I(\mathbf{r},z)\nabla\varphi(\mathbf{r},z)], \qquad (1)$$

where $I(\mathbf{r},z)$ is the intensity in a position r in a plane placed at z in the direction of the propagation. k stands for $\lambda/2\pi$, while $\varphi(\mathbf{r},z)$ is the phase of the wavefront at each position. For two close planes, P_1 and P_2, separated Δz from the pupil plane P_0, it can be derived[6] from Eq. (1) that

$$\frac{I_1 - I_2}{I_1 + I_2} = -\frac{\Delta z}{k}\left[\nabla^2\varphi(\mathbf{r},z_0) + \delta(e)\frac{\mathrm{d}}{\mathrm{d}\mathbf{n}}\varphi(\mathbf{r},z_0)\right]. \qquad (2)$$

A first-order approximation of $I(\mathbf{r},z)$ has been applied, that is, it is assumed to be a linear variation of the intensity in one given point between the two planes. This is always true for very close planes or for not very aberrated wavefronts. The term on the left-hand side of Eq. (2) corresponds to the point-to-point contrast between the two images. This can be considered as the sensor's signal (S). Equation (2) describes the relationship between S and the phase in the pupil plane $[\varphi(\mathbf{r},z_0)]$. As can be seen, in the signal, there are two different types of phase information. The first refers to the curvature of the wavefront, while the second corresponds to its first derivative in the direction of light propagation (unit vector $\mathbf{n}$). The Dirac delta function $\delta(e)$ limits the contribution of the latter term only to points at the pupil's edge.

The phase retrieval from S corresponds to a Laplacian resolution with Neumann boundary conditions. Several numerical methods have been developed to solve this problem. The most common ones are those based on iterative Fourier transform algorithms,[9] taking into account the fact that, in Fourier space, the second derivative corresponds to a simple division by the angular frequency square (w^2). A scheme of the Gershberg-type algorithm[9] that we have used is depicted in Fig. 1. A first estimation of the phase is achieved by applying the Fourier transform to S, dividing the result by w^2, and finally computing the inverse transform. The second term in Eq. (2), which corresponds to the first derivative contribution, has not been taken into account, so this initial solution is incorrect. The Neumann boundary condition is then imposed, making $\mathrm{d}\varphi/\mathrm{d}\boldsymbol{n}$ null within a narrow band around the signal's edge. S is then recalculated, restoring the original signal inside the new boundaries. The whole process is then iterated until the phase estimation converges.

0146-9592/06/152245-3/$15.00

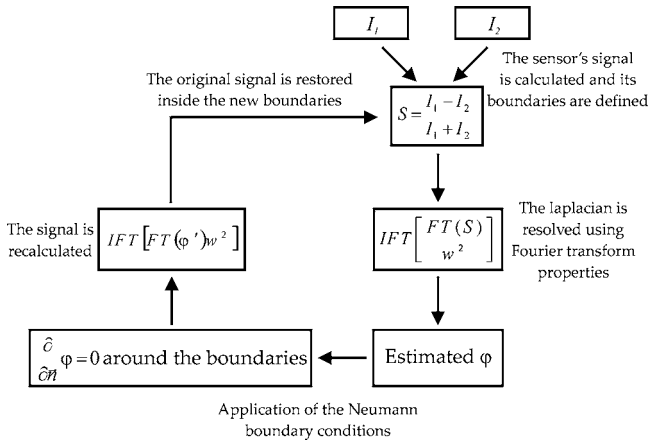

Fig. 1. Scheme of the algorithm used for wavefront retrieval from the captured images.

Although the determination of the wavefront using the curvature sensor generally has a higher time cost than techniques currently used in ocular optics studies, the sampling of the pupil, in general, will be much higher, due to the direct recording of the pupil image. Much finer details may potentially be detected, which would make it possible to determine the contribution of high-order aberrations, missed by current methods. Depending on the system's design, a great dynamic range could also be achieved, avoiding the effect of cross talk between microlenses in the H–S sensor. Moreover, due to its simplicity, the system's implementation is much more cost effective.

The experimental setup, schematized in Fig. 2, corresponds to a classical double-pass system, adapted to capture the two defocused images of the pupil. A fiber-coupled infrared laser diode (LD) ($\lambda=780$ nm) is used as a light source, collimated by lens L1 ($f=100$ mm). A 1 mm diaphragm (D) is placed so that a narrow beam enters the eye. This beam is projected on the subject's retina, slightly scanning the position around the fovea using a rotating mirror (SM). This scanning reduces the speckle noise present in the images. Although the sensor can accurately measure large amounts of defocus, a Badal system that compensates for the subjects' spherical refraction is placed in the returning path [achromatic doublets L3, L4 ($f=100$ mm) and a motorized stage with mirrors M2 and M3], which compensates for the subjects' spherical refraction. Therefore the wavefront is flatter as it travels through the optical setup. In this way, the aberrations introduced by the whole system are reduced as much as possible. The images are captured by CCD1, a conventional 8-bit CCD camera (Hamamatsu C7500) with improved sensitivity in the near-infrared range. An afocal system formed by lenses L5 ($f=75$ mm) and L6 ($f=25$ mm) is used to image them. The subject views a fixation target (FT, collimated by lens L2, with $f=75$ mm) at infinity to avoid accommodative effects and undesirable eye movements while the measurements are being taken. Finally, a camera (CCD2) focused on the subject's pupil helps in its positioning.

To ensure that both images are captured at the same time, we have implemented a system that splits the light coming out of the eye into two beams (which is referred to as the "Splitter" in Fig. 2, and is schematized in detail on the left-hand side of this figure). The reflected beam coming from a 50/50 beam splitter (BS 4) is redirected by mirrors M6, M7, and M8. Thus two parallel beams are obtained, separated by 10 mm, and with a 33 mm difference in the optical path. By focusing the CCD camera on a plane 16.5 mm before the subject's pupil conjugate plane, we obtain both defocused pupil images in the same capture, one on the right-hand side of the image and the other on the left-hand side.

To evaluate the various design possibilities, the methodology of the measurements and the phase retrieval algorithms, we performed a complete set of computer simulations. This helped us to analyze important aspects, such as the optimal placement of the detection planes or the impact of the camera's noise levels, which affect the performance of the system, ensuring in this way a good performance throughout the range of aberrations of interest in the study of ocular optical quality. Regarding the design process, we focused our efforts on minimizing the system's aberrations, while maximizing the sensor's dynamic range and sensitivity. For example, primary astigmatisms from 0.05 to 11.0 diopters can be retrieved within a range of error of 3% for the 16.5 mm displacement of the detection planes that were finally considered.

We tested the performance of the sensor by carrying out a complete set of the artificial eye's measurements. This artificial eye consisted of a short focal length lens acting as the eye's optics and a diffuser acting as the retina. To test different pupil size conditions, we placed a diaphragm wheel in front of the eye, in the plane where the subject's pupil should be located. We checked the performance of the system by placing different trial lenses (both spherical and cylindrical) in front of the artificial eye and by comparing the aberration obtained with its nominal value. Figure 3 clearly shows that our results correlate very well with the theoretical values. Apart from

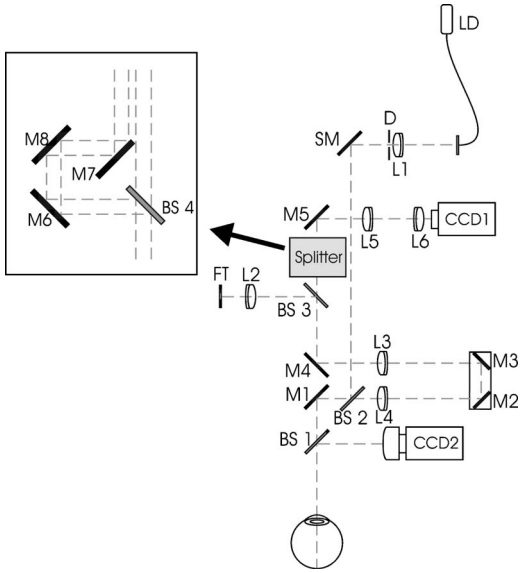

Fig. 2. Experimental setup.

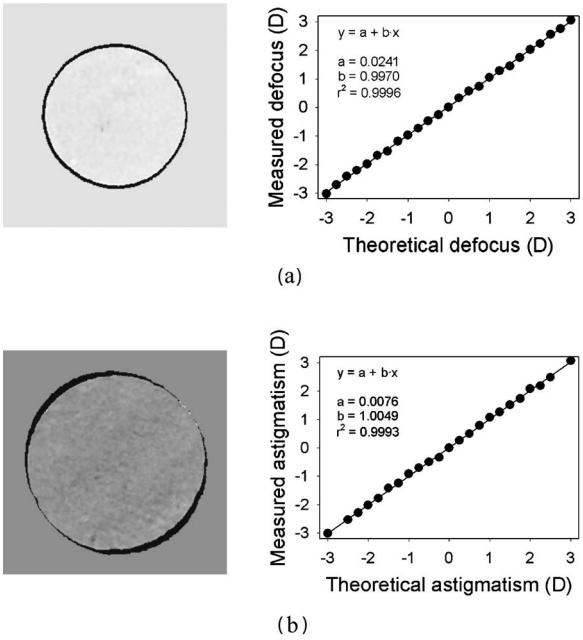

Fig. 3. Results obtained for different trial lenses: (a) spherical lenses (4 mm pupil), and (b) cylindrical lenses (5 mm pupil). Examples of the sensor signals (S) for each case are shown on the left-hand side. The correlation between our results and the nominal value of the lenses is shown on the right-hand side.

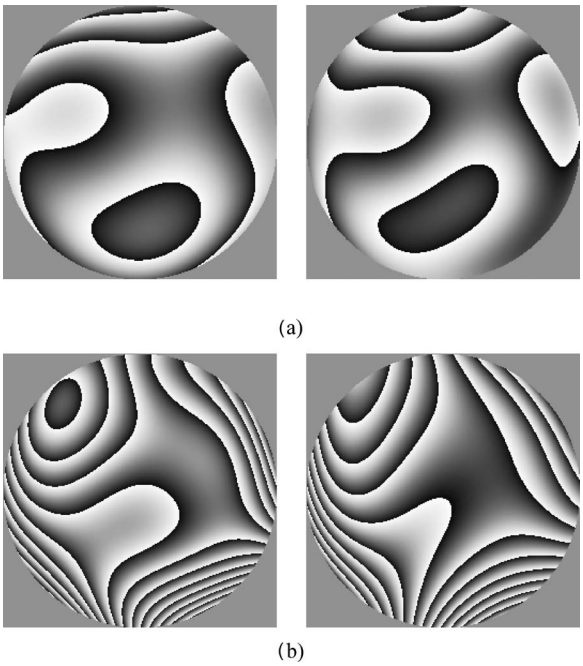

Fig. 4. Wavefront estimations from H–S (left) and curvature (right) sensors for (a) low aberrated eye, (b) more aberrated eye.

defocus or astigmatism, we obtained a small contribution of the rest of the terms, which affected the wavefront in a mean rms of 0.016 ± 0.007 μm (adjusting up to sixth Zernike order with a pupil size of 5 mm). This residual aberration consistently increases with the power of the measured lens, so we assume that it is mainly caused by the aberrations of the system. Another possible reason is that speckle noise is not completely removed from the images. Changing the pupil size does not dramatically affect the accuracy of the sensor. As an example, for a 2 diopter spherical trial lens, we obtained 1.996 diopters for 4 mm, 1.978 diopters for 5 mm, and 1.956 diopters for 6 mm. Error increases with pupil size, which confirms that the system's aberrations do play a role but are not critical.

Finally, we compared H–S and curvature sensor measurements for different eyes. Regarding the curvature sensor measurements, four images were sequentially captured for each eye in our CCD at 400 ms/frame. A background image was also registered and subtracted from the pupil images. The H–S measurements were performed using a system developed by us. The microlens array was composed of lenses that were 0.2 mm in diameter and whose focal length was 6.3 mm. An afocal 1/2 magnification system images the pupil on this microlens array, so a 5 mm pupil is sampled by 123 lenses. We captured five 160 ms/frame consecutive measurements for each eye, considering the mean wavefront. Figure 4(a) shows an example of the results obtained for a low aberrated eye (rms = 0.33838 μm, measured with H–S and not taking into account the defocus term). As can be seen, the wavefront estimations are very close to each other, with a difference in rms of 0.0059 μm. For a more aberrated eye (rms = 1.31882 μm), shown in Fig. 4(b), the rms difference is larger, 0.056 μm, although it is still in the order of the variability between the measurements taken using the two techniques.

In conclusion, we have developed a curvature wavefront sensor adapted for ocular aberration determination. The preliminary results show a performance similar to that of the most commonly used sensors. Future research, including postsurgery eye measurements, will show the full potential of this technique for estimating high-order aberrations.

Fernando Díaz-Doutón (diaz@oo.upc.edu) and Sergio Oscar Luque thank, respectively, the Ministerio de Educatión y Ciencia (Spain) and the Generalitat de Catalunya (Spain) for the Ph.D. grants they have received.

References

1. R. Navarro and E. Moreno-Barriuso, Opt. Lett. **24**, 951 (1999).
2. J. Liang, B. Grimm, S. Goelz, and J. F. Bille, J. Opt. Soc. Am. A **11**, 1949 (1994).
3. P. M. Prieto, F. Vargas-Martin, S. Golez, and P. Artal, J. Opt. Soc. Am. A **17**, 1388 (2000).
4. F. Diaz-Douton, A. Benito, J. Pujol, M. Arjona, J. L. Guell, and P. Artal, Invest. Ophthalmol. Visual Sci. **47**, 1710 (2006).
5. C. Roddier and F. Roddier, J. Opt. Soc. Am. A **10**, 2277 (1993).
6. F. Roddier, Appl. Opt. **29**, 1402 (1990).
7. F. Roddier, Appl. Opt. **27**, 1223 (1988).
8. S. Gruppetta, L. Koechlin, F. Lacombe, and P. Puget, Opt. Lett. **30**, 2757 (2005).
9. F. Roddier and C. Roddier, Appl. Opt. **30**, 1325 (1991).